THREE-DIMENSIONAL UNIT SLUG IN A HORIZONTAL PIPELINE

Conference Paper · June 2010

CITATIONS
6

READS
59

5 authors, including:

Mijail Febres
Institut de Mécanique des Fluides de Toulouse
8 PUBLICATIONS **12** CITATIONS
SEE PROFILE

Angela Nieckele
Pontifícia Universidade Católica do Rio de Janeiro
106 PUBLICATIONS **539** CITATIONS
SEE PROFILE

Roberto Fonseca Jr
Petróleo Brasileiro S.A.
17 PUBLICATIONS **82** CITATIONS
SEE PROFILE

Three-dimensional Unit Slug in a Horizontal Pipeline

M. Febres*, A.O. Nieckele*, R. Fonseca Jr.† and L.F.A. Azevedo*

* Department of Mechanical Engineering, PUC/Rio, Rio de Janeiro, RJ, 22453-900, BRAZIL
† Petrobras, R&D Center, Rio de Janeiro, RJ, 21941-915, BRAZIL
mijail_febres@aluno.puc-rio.br, nieckele@puc-rio.br, robertofonseca@petrobras.com.br, lfaa@puc-rio.br

Keywords: Slug flow; horizontal pipeline; three dimensional, VOF; PIV

Abstract

Among all possible flow configurations that multiphase flow can take, the slug flow regime plays an important role because of its intermittent characteristics and its strong pressure gradients in pipelines, where this flow regime can be found. Due to its importance, several papers can be found in the literature. Although, the available works provide useful data, there are still missing relevant information of random gas-liquid characteristics, structures evolution and interaction along the pipeline. In the present work, a detailed numerical and experimental study of a slug flow in a horizontal pipeline is performed. The 3-D isothermal flow field was numerically determined with the finite volume method. The Volume of Fluid (VOF) model was employed to determine the interface of a single unit slug, obtained by employing a coordinate system coincident with the Taylor bubble. The turbulence was modeled with the RNG κ–ε model. The numerical predictions of the bubble shape, velocity profile and translation slug velocity were compared with the measured data, obtained with the PIV and Laser Doppler techniques. Good agreement was obtained between the predicted and measured data.

Introduction

Multiphase flow is very common in the petroleum industry. Not only different fluids, such as oil and water, can be found, but these fluids can be present in different phases (liquid or gas). Further, during its transport, depending on the phase's superficial velocities, different flow patterns can be found, such as "smooth stratified", "wavy stratified", "elongated bubble", "slug", "annular", "chaotic", "bubble", etc.

Numerical simulation has became a very important tool to predict multiphase flow inside pipelines due to the worldwide increasing fuel demand for industry, as well as higher standard requirements for equipment design for petroleum processing and transport. For an efficient equipment or pipe design, it is desired to determine the individual hydrodynamic characteristics of each flow pattern, such as pressure drop and flow intermittence parameters.

One of the most common flow patterns during operation in Petroleum processing facilities is the "slug" pattern. There have been many attempts in the literature to model a two-phase slug flow. One of the first models, presented by Wallis (1969), is based on the concept of the single unit slug with a reference frame moving with the tip of the bubble. Later, Taitel and Barnea (1989) using the same concept, divided the single unit slug into two parts: the liquid slug and the liquid film zones. Fagundes Netto et al. (1999) developed a model based on mass and momentum conservation equations to predict the shape of the tip and tail of the gas bubble, as well as the liquid slug, and presented a comparison with experimental data.

Taitel et al. (2000) showed that a negative pipe inclination damps slug formation. Orell et al. (2004) used a sub-model of Taitel and Barnea (1990) model, and obtained an increase of the pressure loss, obtaining good results in agreement with experimental data. De Freitas et al. (2008) applied the single unit slug concept through a vertical pipe and studied the effect of gas expansion. Several codes have been developed and are widely used, such as PLAC (Black et al., 1990) and OLGA (Bendiksen et al., 1991).

A literature search reveals a large number of papers presenting experimental investigations of the global characteristics of slug flows. These experiments were conducted to support the development and verification of slug flow models in the horizontal configuration. In these studies, the focus is on global measurements such as pressure drop, overall void fraction and statistical parameters such as slug length distribution, slug frequency and film thickness (e.g., Bendiksen, 1984, Cook and Behnia, 2000, Bertola, 2002). Probably due to the complex nature of the slug flow pattern, relatively few papers were found reporting results on detailed measurements of the flow field in the liquid slug and film layer under the gas bubble. Detailed information on the flow behavior is critical to the proper understanding of the physical mechanisms governing the flow.

Instantaneous full field measurements of the liquid phase in slug flow were reported by Carpintero-Rogero et al. (2006). The authors employed three simultaneous optical techniques to produce time-averaged and turbulent data for the liquid slug and film layer: PIV (Particle Image Velocimetry), LIF (Laser Induced Fluorescence) and PST (Pulsed Shadow Technique). These same techniques were employed in the present paper.

Recently, Wang et al. (2007) experimentally showed

that the translational velocity varies with the distance from the entrance. It was also shown that the slug frequency is a function of the liquid superficial velocity.

Although, the available works provide useful data, there are still missing relevant information of random gas-liquid characteristics, structures evolution and interaction along the pipeline.

Among the several techniques to numerically predict the slug pattern, the Two Fluid Model, introduced by Ishii (1975), is a very successful one, since it does not require the introduction of transition criteria between flow patterns. However, it does require the definition of interface transfers.

Issa e Kempf (2003) presented a one-dimensional formulation based on the two fluid model to predict the slug formation and Ortega and Nieckele (2005) investigated the model performance with a conservative and non-conservative formulation.

Detailed slug flow information can be obtained with 2D or 3D simulations, however those are very expensive. Thus, to reduce the cost, most available work considers a single slug unit. Cook et al. (2001) investigated an air bubble in stagnant water using VOF, in symmetrical 3D domain with several inclination angles (5° to 75°), and obtained good agreement with experimental data. Taha Taha et al. (2006) and Ujang et al (2008) applied the VOF model to simulate the slug flow with a reference frame moving with the bubble. While the former considered a symmetrical 2-D and 3-D vertical pipe, the later investigated a horizontal slightly inclined slug flow. Ujang et al. (2008) showed a tendency of the slug nose to move in direction of the pipe center line.

Vallée et al (2008) using ANSYS CFX, simulated air/water stratified and slug flow in a square pipe, obtaining good qualitative results.

In the present work, the commercial CFD software FLUENT™ was employed to solve numerically the air/water two-phase slug flow with the single unit slug approach. The slug translational velocity and film velocity profiles were compared with measured data, presenting good agreement.

Nomenclature

C	empirical constant
D	diameter (m)
F	external force per unit volume (N/m^3)
Fr	Froude number
g	gravitational constant (m/s)
G	turbulent generation term (Pa/s)
L	length (m)
n	normal direction
p	pressure (N/m^2)
S	mean deformation rate (1/s)
$\vec{u}$	velocity vector (m/s)
V	vertical velocity (m/s)
W	axial velocity (m/s)

Greek letters

α	volume fraction
ε	turbulent dissipation rate (m^2/s^3)
κ	turbulent kinetic energy (m^2/s^2)
λ	inverse of Prandtl number
μ	viscosity (Pa s)
$\Re$	interface curvature (1/m)
ρ	specific mass (kg/m^3)
σ	surface tension (N/m)

Subscripts

ef	effective
g	gas
ℓ	liquid
m	mixture
s	superficial velocity
t	turbulent

Mathematical Model

To determine the two-phase slug flow field inside a horizontal pipeline, the VOF (volume of fluid) model (Hirt and Nichols, 1981) was selected. The VOF model is based on the solution of one single set of conservation equations of mass and momentum. An auxiliary variable, named "volume fraction" α_i, is considered to identify the region occupied by each phase. All variables and properties fields are shared by both phases, and they represent average values. Properties and variables on each cell are entirely representative of one phase or a mixture of the phases depending on the value of volume fraction, which are defined as follows: $\alpha_i = 0$ if the cell does not contain fluid "i", $\alpha_i = 1$ if the cell is full of fluid "i" and $0 < i < 1$ if the cell contains the interface between the phases. The sum of volume fractions is equal to 1, i.e., $\alpha_g + \alpha_\ell = 1$.

Properties, like density ρ and viscosity μ, which appear in transport equations, are evaluated by taking in account the amount of each phase in the cell, as follows: $\rho = \alpha_g \rho_g + \alpha_\ell \rho_\ell$; $\mu = \alpha_g \mu_g + \alpha_\ell \mu_\ell$.

The interface tracking is determined by assuming a material derivative of the interface equal to zero for a referential on the interface, thus

$$\frac{\partial \alpha_g}{\partial t} + \vec{u} \bullet \nabla \alpha_g = 0 \tag{1}$$

where $\vec{u}$ is the time average velocity vector.

The Reynolds average continuity and momentum conservation equations can be written as

$$\frac{\partial}{\partial t}(\rho \vec{u}) + \nabla \bullet (\rho \vec{u}) = 0 \tag{2}$$

$$\frac{\partial}{\partial t}(\rho \vec{u}) + \nabla \bullet (\rho \vec{u}\,\vec{u}) = -\nabla p + \rho \vec{g} + \nabla \bullet [\mu_{ef}\ 2\underline{\underline{S}}] + \rho \vec{g} + \vec{F} \tag{3}$$

where p is the pressure, $\vec{g}$ is the gravity acceleration vector, $\mu_{ef} = \mu + \mu_t$ is the effective viscosity, μ_t is the turbulent viscosity, $\underline{\underline{S}}$ is the mean rate of strain tensor and $\vec{F}$ is an external force which takes in account the effects of surface tension ($\sigma_{g\ell}$) of two phases and it is based on the CSF model (Continuum Surface Force) developed by Brackbill *et al.* (1992)

$$\underline{\underline{S}} = \frac{1}{2}(\nabla \vec{u} + \nabla \vec{u}^T); \quad \vec{F} = \sigma_{g\ell} \frac{\rho \Re \nabla \alpha_g}{(\rho_g + \rho_\ell)/2} \tag{4}$$

where the interface curvature $\Re = \nabla \bullet \hat{n}$ is determined as a

function of the volume fraction gradient in cells that contains the interface ($\hat{n} = \vec{n} / |\vec{n}|$ where $\vec{n} = \nabla \alpha_g$).

Turbulence was taken into account with the κ–ε RNG model (Yakhot et al., 1992). For high Reynolds number, the turbulent viscosity is

$$\mu_t = C_\mu \, \rho \, \kappa^2 / \varepsilon \quad ; \quad C_\mu = 0.0845 \tag{5}$$

where κ is the turbulent kinetic energy and ε its dissipation rate, and are obtained from the following transport equations:

$$\frac{\partial}{\partial t}(\rho \, \kappa) + \nabla \bullet (\rho \, \vec{u} \, \kappa) = \nabla \bullet [\lambda_\kappa \, \mu_{ef} \nabla \, \kappa] + G_\kappa - \rho \, \varepsilon \tag{6}$$

$$\frac{\partial}{\partial t}(\rho \, \varepsilon) + \nabla \bullet (\rho \, \vec{u} \, \varepsilon) = \nabla \bullet [\lambda_\varepsilon \, \mu_{ef} \, \nabla \, \varepsilon] + C_{1\varepsilon} \frac{\varepsilon}{\kappa} G_\kappa - C_{2\varepsilon}^* \rho \frac{\varepsilon^2}{\kappa} \tag{7}$$

In these equations, G_κ represents the generation of turbulence kinetic energy due to the mean velocity gradients

$$G_\kappa = \mu_t \, S^2 \quad ; \quad S = \sqrt{2 \, S_{ij} \, S_{ij}} \tag{8}$$

λ_k and λ_ε are the inverse Prandtl numbers for κ and ε respectively, obtained from the following expressions:

$$\left| \frac{\lambda_{\kappa,\varepsilon} - 1.3929}{\lambda_o - 1.3929} \right|^{0.6321} \left| \frac{\lambda_{\kappa,\varepsilon} + 2.3929}{\lambda_o + 2.3929} \right|^{0.3679} = \frac{\mu}{\mu_{ef}} \tag{9}$$

The destruction of ε depends on $C_{2\varepsilon}^* = C_{2\varepsilon} + R_\varepsilon^*$, where

$$R_\varepsilon^* = \frac{C_\mu \, \eta^3 (1 - \eta / \eta_0)}{1 + \beta \, \eta^3} \quad ; \quad \eta = S \frac{\kappa}{\varepsilon} \tag{10}$$

The empirical constants are: $C_{1\varepsilon} = 1.42$, $C_{2\varepsilon} = 1.68$, $\lambda_o = 1$, $\beta = 0.012$ and $\eta_0 = 4.38$.

Boundary conditions: To predict a single unit cell, a reference frame moving with the bubble was employed. Therefore, at the pipe wall a slug translational velocity was prescribed. At the entrance of the domain, the mixture velocity was imposed as $W_m = w_{s\ell} + w_{sg}$, where $w_{s\ell}$ and w_{sg} are the liquid and gas superficial velocities, relative to the wall. The entrance turbulent quantities were

$$\kappa = \frac{3}{2}(W_m \, \zeta)^2 \quad ; \quad \varepsilon = C_\mu^{3/4} \, \kappa^{3/2} / \ell_c \tag{11}$$

with ζ=0.05 and ℓ_c =0.07 D. At the exit a constant pressure was prescribed.

Experimental Facility

Figure 1 schematically presents the test section constructed to conduct the experiments. A 24mm diameter, 10 meters long Plexiglas pipe was mounted on a rigid steel frame that could be rotated around a pivot to produce inclination angles between 0 and +10° with the horizontal. In the present paper only results for the horizontal cases will be presented. The pipe length-to-diameter ratio was 400, which should be sufficient for the formation of stable slugs. Water from a reservoir was pumped in closed circuit through the test pipe by a progressive cavity pump. A centrifugal blower provided compressed air for the test section. Calibrated rotameters were used to measure the water and air flow rates. Air and water were mixed at a Y-junction positioned at the entrance of the Plexiglas pipe. After passing through the test pipe, the two-phase mixture returned to the reservoir where a tangential inlet aided the phase separation process. The green and blue arrows in Fig. 1a indicate, respectively, the water and air flow paths in the test section.

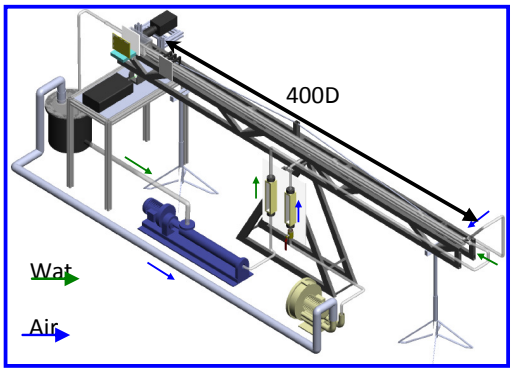

(a) overview of test section

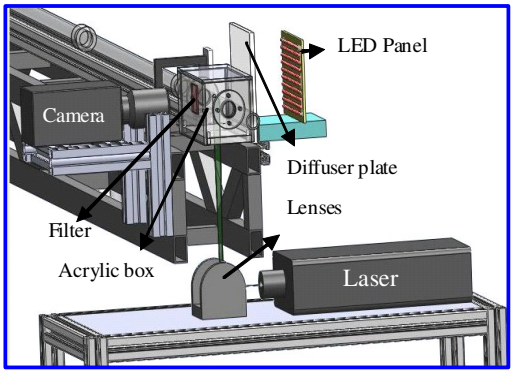

(b) Components of the measuring system

Figure 1: Experimental apparatus.

The measuring section was located at 350 diameters from the pipe entrance. As it can be seen schematically in Fig.1b, the measuring section was specially prepared to receive the components necessary for the implementation of the three optical techniques employed in the experiments, namely, PIV, LIF and PST. Light from a double cavity, 120-mJ, Nd-YAG laser manufactured by New Wave was shaped into a plane sheet and directed to the meridional vertical plane of the pipe. A set of cylindrical and spherical lenses was used to form the light sheet that presented approximate dimensions in the measuring region of 50 × 0.5 mm (width × thickness). A 45° mirror was also employed to divert the laser beam that entered the test section from below, as indicated in the figure. In order to minimize reflections from the laser light at the curved pipe surface, a rectangular glass box was mounted around the pipe at the measuring area. The box was filled with water. The maximum firing frequency of each laser cavity was 15 Hz. The dual cavity laser system allows for very short pulse

intervals between laser firing. Typical pulse intervals of the order of micro seconds can be easily achieved, which is adequate for measuring liquid velocities significantly higher than the levels encountered in the experiments conducted. The laser was operated to emit green light at a wavelength of 532 nm. The particle images were acquired by a PIVCAM 10-30 digital camera manufactured by TSI. The camera can be operated in the frame straddling mode, which allows for the capture of pairs of consecutive images with time intervals in the micro second range. Pairs of consecutive images can be acquired by the camera at 15 Hz, which is compatible with the laser firing frequency. The camera offered a 1000 x 1000 pixel resolution. As indicated in the figure, the camera was mounted orthogonally to the light sheet plane. A 50-mm focal distance lens was used in the experiments. The panel of LED's for the background illumination required by the PST technique was mounted on the opposite side of the camera. A sand-blasted diffuser glass plate was positioned in front of the LED panel to improve the spatial uniformity of the background illumination. The high-pass optical filter required for the LIF technique was fixed on the rectangular glass box in the viewing path of the camera. In the present study seeding was obtained with the use of 15-μm-diameter fluorescent particles with peak excitation wavelength at 542 nm and peak fluorescence emission at 612 nm. The particles density was 1.05 g/cm^3.

A photogate cell was installed around the pipe, upstream of the glass box. This cell (not shown in the figure) provided trigger signals for the velocity measuring system. The cell output a high voltage signal when gas passes through the cell, and a low voltage signal when water is flowing through. The transition from a high to low voltage signal is an indication of the passage of a gas-liquid interface at the photogate position. A controlling circuit triggered by the photogate signal outputs a trigger signal to the velocity measuring system after a pre-set time delay. By controlling the time delay, it was possible to always measure the liquid velocity field at a pre-determined position in relation to the gas bubble surface position. A second photogate cell was installed at a known position from the first one and was employed in the measurement of statistical slug properties, such as length, frequency and velocity distributions.

Numerical Scheme

To solve the mathematical model, the commercial software FLUENT™ was employed. It is based on the Finite Volume technique which consists on dividing the computational domain on small control volumes and integrating spatially and temporarily the transport equations over them. First order implicit technique was used for the time integration, while the spatial integration was handled with the second order "QUICK" scheme (Leonard, 1979).

The pressure-velocity coupling was solved with the PISO algorithm (Issa, 1986) and PRESTO was selected as the interpolation scheme for pressure.

To reconstruct the interface of the VOF methodology, the "Geometric Reconstruction" technique was applied.

The resulting discretization algebraic equations were solved using the AMG (*Algebraic Multigrid Solver)* option (Hutchinson et al., 1986).

Computational domain. The mesh of the circular pipe was generated with GAMBIT™. Solution was obtained with 5100, 29000 and 232.000 control volumes in the cross section, and the intermediate mesh illustrated in Fig. 2a was selected, since the difference in the velocity profile was inferior a 0.5%. Similar test was performed for the axial position and 100 control volumes were selected with the mesh concentrated in the region indicated in the Fig. 2c, with length equal to 2D. At this region, where the tip of the bubble was located, the mesh was approximated uniform in the axial direction (Fig. 2b).

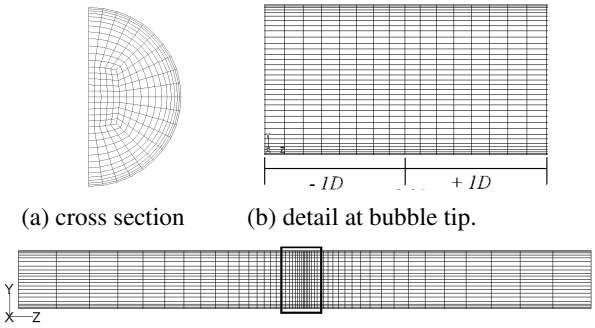

(a) cross section (b) detail at bubble tip.

(c) transversal section

Figure 2: Mesh distribution.

Initialization. The initial condition was defined according to Ujang et al. (2008), in which water volume fraction was set as "1" at first half of the pipe and equal to "0" at the second half (Fig.3).

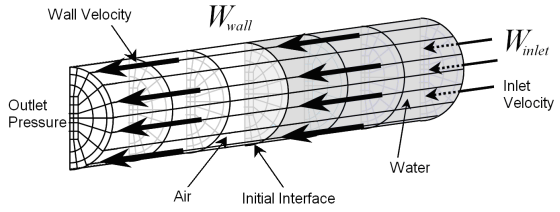

Figure 3: Boundary conditions and domain initialization.

The wall velocity was initialized according to Bendiksen (1984) models to estimate the slug translational velocity

$$W_T = C_o\, W_m + W_{drift} \quad ; \quad W_{drift} = C_1\sqrt{g\, D} \qquad (12)$$

where C_o stands for the distribution parameter of distribution,

$$\begin{matrix} C_o = 1.05 \Rightarrow Fr_c < 3.5 \\ C_o = 1.20 \Rightarrow Fr_c \geq 3.5 \end{matrix} ; Fr_c = \frac{w_{sl}}{\sqrt{g\, D}} ; \; C_1 = 0.54 \quad (13)$$

g is the gravity acceleration, D the pipe diameter and Fr_c stands for the critic Froude number.

The wall velocity obtained with the correlation given by Eq. (12) and coefficients of Eq. (13) was a good estimated, but it was corrected based on the flow field, so that the bubble position was maintained fix inside the computational domain. Usually three iterations were necessary to find a still bubble.

Figure 4 illustrates the bubble position inside the domain at different time instants. Figure 4a corresponds to the initial wall velocity prescribed from Eqs. (12) and (13),

and Fig. 4b illustrates the bubble position after the converged wall velocity (translation bubble velocity) was obtained.

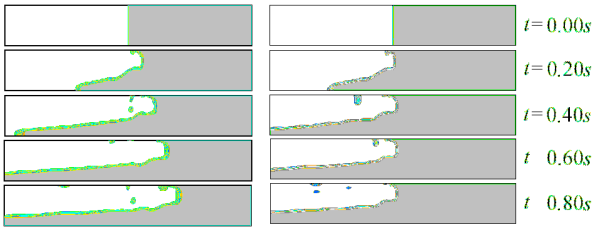

(a) Wall velocity. Eq. (12) (b) Converged wall velocity

C_o=1.05, C_1=0.54

Figure 4: Time evolution of Taylor bubble.

Results and Discussion

It was considered a pipeline with the same diameter as in the experimental apparatus (D = 0.024m). The length was set as L = 25D, long enough to capture one single bubble and a fully developed liquid slug). The working fluids were air and water (air: ρ_g=1.225 kg/m^3, μ_g= 1.790×10^{-5} Pa s; water: ρ_ℓ=998.2 kg/m^3, μ_ℓ= 1.003×10^{-3} Pa s, $\sigma_{g\ell}$=0.073 N/m).

Six combinations of gas and liquid superficial velocities were examined. Table 1 presents the superficial velocity of each phase, the resulting mixture velocity, and the superficial velocities ratio.

The initial slug translational velocity (Eqs. 12 and 13) and the converged wall velocity were also included in Table 1. For all cases tested Fr_c was smaller than 3.5, and the constants from Eq. (13) were: C_o =1.05 and C_1=0.54. The slug translation velocity and the converged wall velocity presented a variation from 5% to 11%. Therefore, a linear regression of the numerical data for the converged slug translation velocity was performed and the coefficients C_o and C_1 of Eq. (12) were re-evaluated. The corrected coefficients based on the numerical solution were: C_o =1.116 and C_1=0.202 (W_{drift}=0.098 m/s). These values are within the range observed experimentally by Bendiksen (1984) for a pipe with 0.0242 m diameter ($1.009 \le C_0 \le 1.188$ and $-0.004\text{m/s} \le W_{drift} \le 0.181\text{m/s}$), indicating that the present VOF solution was capable of predicting drift velocity of a slug two phase flow.

Table 1: Test cases.

Cases	w_{sg} (m/s)	w_{sl} (m/s)	W_m (m/s)	w_{sg}/w_{sl}	W_T	W_{wall} (m/s)
1	0.475	0.295	0.770	1.610	1.071	0.956
2	0.475	0.393	0.868	1.209	1.174	1.067
3	0.475	0.516	0.991	0.921	1.303	1.205
4	0.788	0.295	1.083	2.671	1.399	1.308
5	0.788	0.393	1.181	2.005	1.502	1.416
6	0.788	0.516	1.304	1.527	1.631	1.552

The six cases selected to be tested were located inside a pattern map (Fig. 5) where it can be seen that three of them are in the elongated bubble region and the other three are at the interface of the elongated bubble region with the slug region.

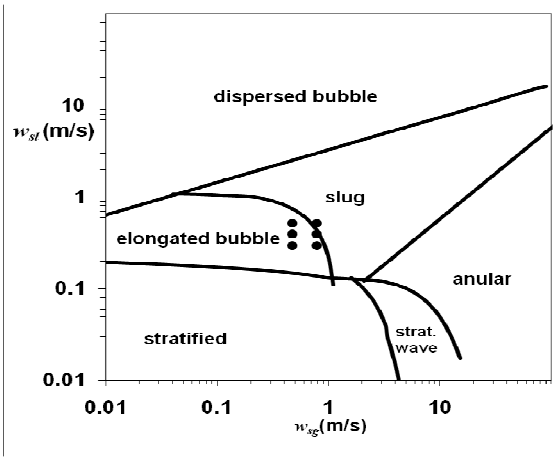

Figure 5: Map pattern

Bubble shape. To illustrate the bubble nose shape, Case 6 was selected. The volume fraction surface equal to zero is plotted on top of the mesh (Fig. 6b) and it is compared with the image obtained experimentally with the combination of laser induced florescent and synchronized background illumination (Fig. 6a). A similar configuration is obtained, where it can be seen that the bubble nose is oriented downward, agreeing with previous experimental observation of Bendiksen (1984). However, the numerical inclination is quite small. Further, the numerical simulation predicted a more round nose than observed experimentally.

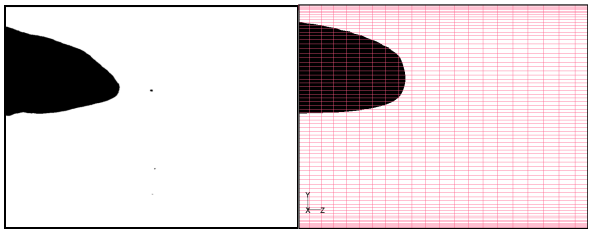

a) Experimental. b) Numerical

Figure 6: Bubble nose shape. Case 6

To visualized the bubble shape, it is shown in Fig. 7, contours of the volume fraction at five cross section for Case 1. The bubble presents an oval cross section, which gets flatter along the bubble length. Note that the bubble is squeezed and pushed to the upper part of the pipeline. It can be also be seen that at z = - 0.8 D, the bubble touches the wall and the liquid film above it disappears.

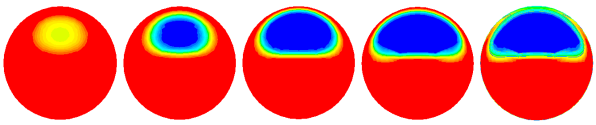

z= 0.0 D z= – 0.2 D z= – 0.4 D z= – 0.6 D z= – 0.8 D

Figure 7: Volume fraction contours at different cross section. Case 1

Velocity field. Figure 8 illustrates a comparison of the measured velocity field with the numerical prediction, for Case 1 and 6, where a reasonable agreement can be observed. It can be seen the inclination of the bubble towards the pipeline center, inducing a maximum velocity dislocated to the center in front of the bubble.

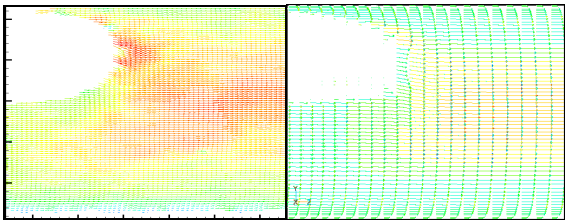

a) Experimental. Case 1 b) Numerical. Case 1

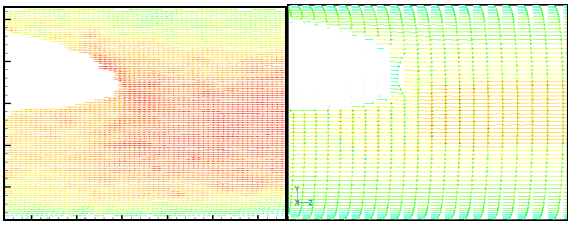

a) Experimental. Case 6 b) Numerical. Case 6

Figure 8: Velocity field. Case 1 and Case 6

Axial velocity profiles were obtained along nine vertical lines located at coordinates from -0.8*D* to 0.8*D* relative to tip of the bubble (0.0*D*), as shown in Fig. 9. The coordinates with negative signal will be called from now on "upstream" and coordinates with positive signal will be called "downstream".

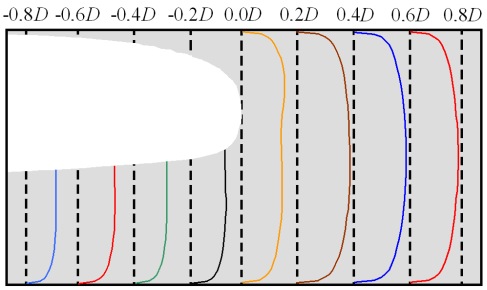

Figure 9: Data Acquisition positions

Detailed results of selected cases are presented here. Figures 10 through 12 show the velocity profiles upstream of the bubble nose, corresponding to the selected Cases 2, 3 and 6, respectively, Figure 13 corresponds to the downstream positions of the three cases. Experimental data is presented with symbols while numerical results are plotted with continuous lines.

Analyzing Figs. 10-12 it can be seen that there is no experimental data in the gaseous phase, because tracing particles were introduce only in the liquid phase. Due to the smaller viscosity, the gas velocity presents a smaller inclination at the wall, leading to much higher velocities than the liquid phase. An excellent agreement between numerical and experimental data was obtained in the liquid region. However, it can be observed a local reduction on the experimental liquid velocity profile near to the interface. This behavior was not predicted numerically, where a smooth transition from the liquid velocity to the gaseous velocity profile is was obtained.

Analyzing Figs. 10-12, it can be seen that the maximum gas velocity increases as one moves upstream, while the maximum liquid velocity diminishes, agreeing with the experimental data.

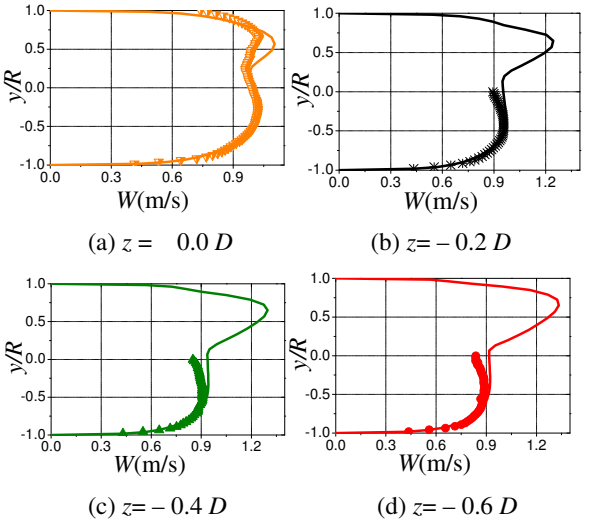

(a) $z = 0.0\ D$ (b) $z = -0.2\ D$

(c) $z = -0.4\ D$ (d) $z = -0.6\ D$

Figure 10: Axial velocity profile, upstream bubble nose. Case 2

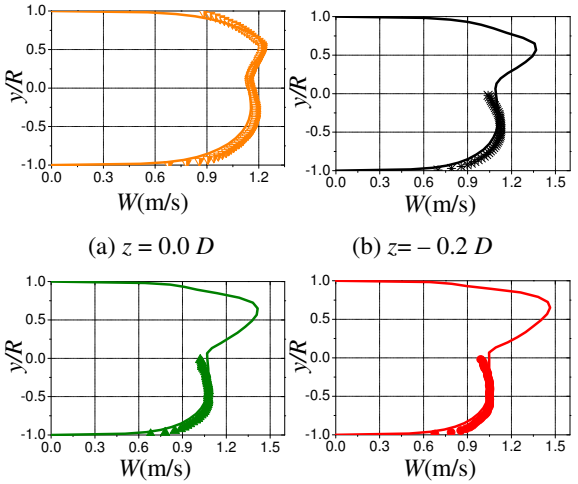

(a) $z = 0.0\ D$ (b) $z = -0.2\ D$

(c) $z = -0.4\ D$ (d) $z = -0.6\ D$

Figure 11: Axial velocity profile, upstream bubble nose. Case 3

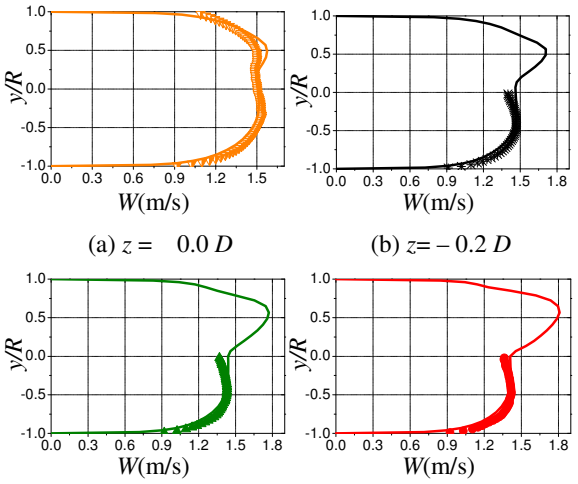

(a) $z = 0.0\ D$ (b) $z = -0.2\ D$

(c) $z = -0.4\ D$ (d) $z = -0.6\ D$

Figure 12: Axial velocity profile, upstream bubble nose. Case 6

The agreement of the numerical results downstream of the Taylor bubble is excellent, as it can be seen in Fig. 13 for the three selected cases. According to several researches like Taitel and Barnea (1990), Polonsky et al (1999) and Shemer (2003), velocity profiles in the liquid slug ahead of the bubble must be fully developed. For all cases tested, this behavior was observed. This information is reinforced in Fig. 14, where velocity profiles for Case 1 corresponding to the tip position and downstream positions from +0.2 *D* through +0.8 *D* are plotted in Fig. 14a. It can be seen that at positions equal to +0.4*D*, +0.6*D* and +0.8*D* the velocity profiles are superimposed indicating a fully developed behavior for velocity ahead of the bubble. Fig. 14b compares the numerical, with experimental and the 1/7 law of fully developed velocity profile, where a good agreement can also be seen.

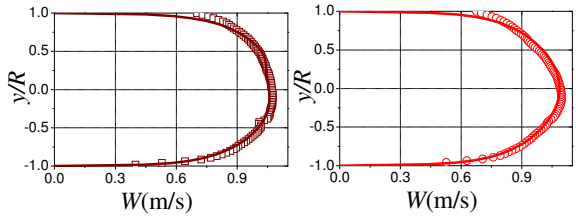

(a) Case 2: z= + 0.2 *D* (b) Case 2: z= + 0.6 *D*

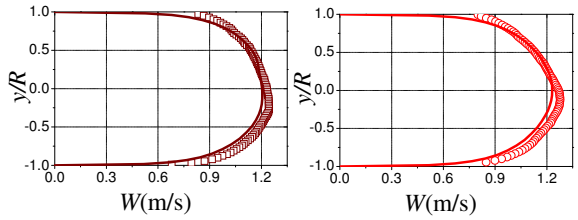

(c) Case 3: z= + 0.2 *D* (d) Case 4: z= + 0.6 *D*

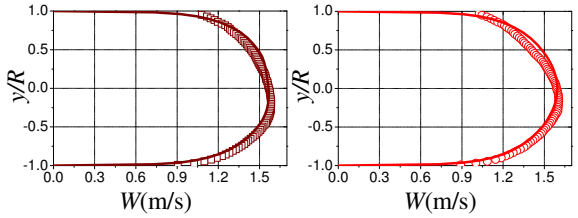

(e) Case 6: z= + 0.2 *D* (f) Case 6: z= + 0.6 *D*

Figure 13: Axial velocity profile, downstream bubble nose.

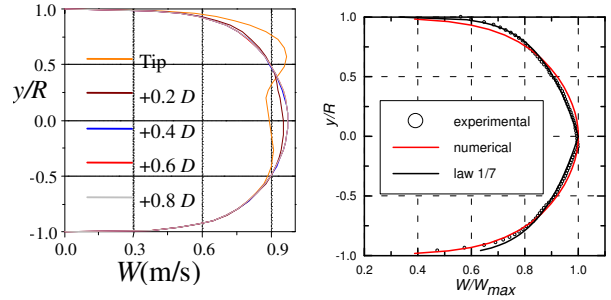

(a) Case 1: several coordinates (b) Case 1: z= + 0.8 *D*

Figure 14: Axial velocity profile, downstream bubble nose.

A comparison between the numerical and experimental velocity profile for the vertical velocity component can be apreciated at Figs. 15 and 16, for Cases 4 and 6, for the upstream and downstream positions, respectively. Once again the numerical model predicted very well the velocity, even though the vertical velocity components are quite small, and more difficult to measure.

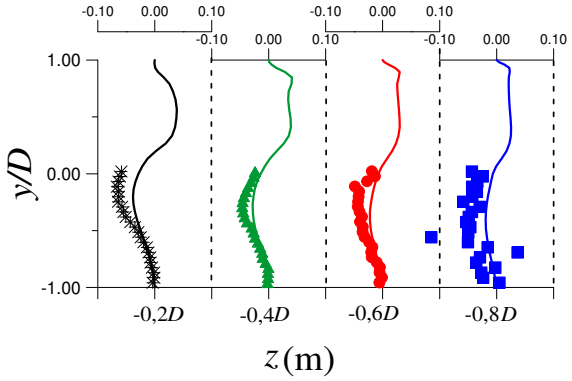

(a) Case 4

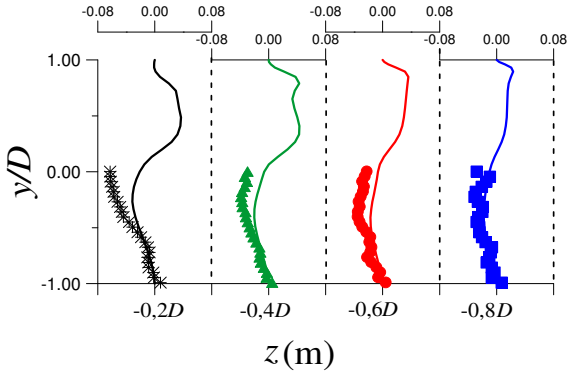

(b) Case 6

Figure 15: Vertical velocity profile, upstream bubble nose

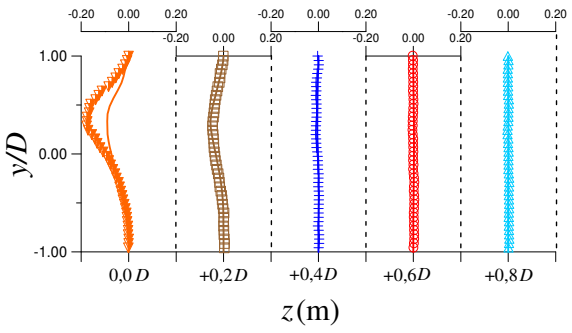

(a) Case 4

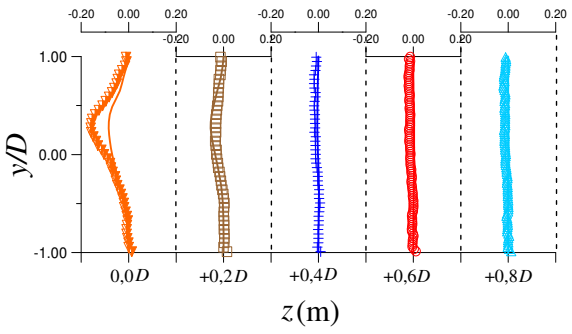

(b) Case 6

Figure 16: Vertical velocity profile, downstream bubble nose

An interesting result to analyze is the velocity field at the pipe cross-section, in the liquid and gas region. Figure 17 illustrates the cross-section velocity vector distribution for Case 1. It can be seen a strong recirculation in the gaseous phase that begins on the interface, climbs to the top of the pipe and returns on the sides. This recirculation is probably responsible for the increase in the bubble diameter as one move upstream of the bubble tip, as shown in Fig. 7.

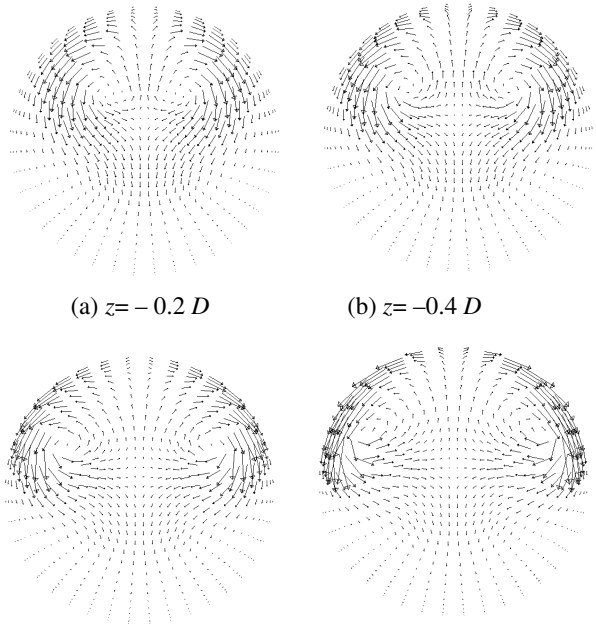

(a) $z = -0.2\,D$ (b) $z = -0.4\,D$

(c) $z = -0.6\,D$ (d) $z = -0.8\,D$

Figure 17: Velocity field at the cross-section, upstream of bubble nose.

To quantify the difference between the velocities measured and numerically determined, a relative error was calculated as

$$Error(\%) = \frac{\sum \left| W_{exp} - W_{num} \right|}{N\, W_m} \times 100 \qquad (14)$$

where N is the number of data, W_{exp} e W_{num}, are experimental and numerical velocities, respectively. The velocity difference was normalized by the mixture velocity W_m. Numerical results are available on each computational nodes and do not necessarily coincide with position where experimental data was measured, therefore, to estimate the error, the numerical data was interpolated for the position where the experimental data was available.

Cases 2, 3 and 6 presented the smallest error for the axial component. At all nine axial positions indicated in Fig. 9, the average error was approximately equal to 5%, while Case 1, 4 and 5 presented an error around 15%.

The vertical component is much smaller than the axial component, thus, a more approximate definition of the error was introduced, as

$$Error(\%) = \frac{\sum \left| V_{exp} - V_{num} \right|}{N \left| V_{exp_{max}} - V_{exp_{min}} \right|} \times 100 \qquad (15)$$

where $V_{exp_{max}}$ and $V_{exp_{min}}$ are the maximum and minimum experimental vertical velocities. As expected the relative error for these components were much higher. The average error was around 20% for all cases.

One possible explanation of the better performance of Cases 2, 3 and 6 can be explained by ratio of the superficial velocities ratio, since these three cases presented the smallest ratio $w_{sg/}\, w_{st}$. This means that if the gas superficial velocity is much higher than the liquid velocity, the performance of the VOF model deteriorates.

Another reason of the discrepancies between the results (although small) can also be attributed to an increase in the dissipation at the interface, which was not modeled, that reduced the liquid velocity at that region, as shown in Figs. 10-12.

Conclusions

Numerical simulation of a single unit slug was performed with the VOF model. The slug translation velocity was obtained and the coefficients of the Bendiksen equation were adjusted to fit all cases. The computed velocity was compared with the experimental data obtained with PIV and Laser Doppler anemometer. It can be said that a very good agreement was obtained.

Acknowledgements

The authors thank CNPq and Petrobras for supporting the development of this work.

References

Barnea, D. & Taitel, Y. Transient Formulation Modes and Stability of Steady-State Annular Flow. Chemical Engineering Science, Vol. 44(2), 325-332 (1989).

Bendiksen, K. H. An Experimental Investigation o f the Motion of long bubbles in inclined pipes. International Journal of Multiphase Flow 10(4), 467-483 (1984).

Bendiksen, K.H.; Malnes, D.; Moe, R.; Nuland, S. The dynamic two–fluid model OLGA: theory and application. SPE Prod. Eng., Vol. 6, 171–180 (1991).

Bertola, V. Slug velocity profiles in horizontal gas–liquid flow, Experiments in Fluids, Vol. 32, pp. 722-727 (2002).

Black, P. S., Daniels, L. C., Hoyle, N. C., Jepson , W. P. Studying Transient Multi-Phase Flow Using the Pipeline Analysis Code (PLAC). Journal Energy Resource Technol., Vol. 112(1), 25 (1990)

Brackbill, J.U., Kothe, D.B., Zemach, C. A continuum method for modeling surface tension. Journal of Computational Physics, Vol. 100(2), 335-354 (1992).

Carpintero-Rogero, E., Kroess, B., Sattelmayer, T. Simultaneous HS-PIV and shadowgraph measurements of gas-liquid flows in a horizontal pipe. 13th Int. Symp. on Applications of Laser Techniques to Fluid Mechanics (2006).

Cook, M. and Behnia, M. Slug length prediction in near horizontal gas-liquid intermittent flow. Chemical Engineering Science, Vol. 55, 2009–2018 (2000).

Cook, M. & Behnia, M. Bubble motion during inclined intermittent flow. International Journal of Heat and Fluid Flow, Vol. 22, 543-551 (2001).

Fagundes Netto, J.R., Fabre, J., Péresson, L. Shape of long bubbles in horizontal slug flow. International Journal of Multiphase Flow, Vol. 25, 1129-1160 (1999).

Hutchinson, B. R. and RAITHBY, G.D. A Multigrid Method Based on the Additive Correction Strategy. Numerical Heat Transfer 9, 511-537, (1986).

Issa, R.I. Solution of the implicitly discretized fluid flow equations by operator-splitting. J. Comput. Phys. 62, 40-65, (1986).

Ishii, M. Thermo–Fluid Dynamic Theory of Two–Phase Flow. Collection de la Direction des Etudes et Researches d'Electricite de France. Eyrolles, Paris, France (1975).

Issa R.I. & Kempf M.H.W. Simulation of slug flow in horizontal and nearly horizontal pipes with the two-fluid model. International Journal of Multiphase Flow, Vol. 29, 69-95 (2003).

Leonard, B. P. A stable and accurate convective modeling procedure based on quadratic upstream interpolation. Comput. Method Appl. Mech. Eng. 19, 59–98 (1979).

Orell A. Experimental Validation of a simple model gas-liquid slug flow in horizontal pipes. Chemical Engineering Science, Vol. 60 (2205) 1371-1381 (2004)

Ortega, A. J. & Nieckele, A. O.Simulation of horizontal two-phase slug flows using the two-fluid model with a conservative and non-conservative formulation, Proceedings of COBEM - Congresso Brasileiro de Engenharia Mecânica. Ouro Preto, MG, Brasil (2005)

Polonsky, S., Shemer, L., Barnea, D. The relation between the Taylor bubble motion and the velocity field ahead of it. International Journal of Multiphase Flow 25, 957–975 (1999).

Shemer, L. Hydrodynamic and statistical parameters of slug flow. International Journal of Heat and Fluid Flow 24, 334–344 (2003).

Taitel, Y. & Barnea, D. Two–phase slug flow. Adv. Heat Transfer, Vol. 20, 83–132 (1990)

Taitel, Y., Sarica, C., Brill, J.P. Slug flow modeling for downward inclined pipe flow: theoretical considerations. International Journal of Multiphase Flow, Vol. 26, 833–844 (2000)

Taha Taha, Z.F. Cui.CFD Modelling of slug flow in vertical tubes. Chemical Engineering Science, Vol. 61, 676-687 (2006).

Ujang, P.M., Pan, L., Manfield, P.D., Lawrence, C.J. and Hewitt, G.F. Prediction of the translational velocity of liquid slugs in gas-liquid slug flow using computational fluid dynamics. Multiphase Science and Technology, Vol. 20(1), 25-79 (2008)

Vallée, C., Höhne, T., Prasser, H., Sühnel, T.. Experimental investigation and CFD simulation of Horizontal stratified two-phase flow Phenomena. Nuclear Engineering and Design, Vol. 238, 637-646 (2008)

Wallis, G.B., 1969. One-dimensional Two-phase Flow, McGraw-Hill, Inc, New York.

Wang X., Guo L. and Zhang X., An experimental study of the statistical parameters of gas–liquid two-phase slug flow in horizontal pipeline. International Journal of Heat and Mass Transfer, Vol. 50, 2439–2443 (2007).